

Dynamical Effects on Sub-barrier Fusion of $^{40,48}\text{Ca}+^{90,96}\text{Zr}$ *

ZHANG Huan-Qiao(张焕乔), LIU Zu-Huan(刘祖华), YANG Feng (杨峰), LIN Cheng-Jian(林承键),
RUAN Ming(阮明), WU Yue-Wei(吴岳伟), LI Zhu-Xia(李祝霞), WU Xi-Zhen(吴锡真),
ZHAO Kai(赵凯), WANG Ning(王宁)

China Institute of Atomic Energy, Beijing 102413

(Received 23 August 2005)

We have measured the fusion cross sections for $^{48}\text{Ca}+^{90,96}\text{Zr}$ around the Coulomb barrier and presented them along with the experimental data of $^{40}\text{Ca}+^{90,96}\text{Zr}$. The experimental results are compared with the improved quantum molecular dynamics model calculations. It is shown in comparison that the dynamical effects play an important role in the sub-barrier fusion reactions.

PACS: 25.70.Jj, 25.70.Gh, 24.10.Pa

The influence of rotation and/or surface vibration of the nuclei in sub-barrier heavy-ion fusion is well studied both experimentally and theoretically in the last one and half decades.^[1-5] It is now realized that heavy-ion fusion in the energy range near and below the Coulomb barrier is strongly affected by degrees of freedom of the interacting nuclei, whose coupling with the relative motion causes a splitting in energy of the single uncoupled fusion barrier. This gives rise to a distribution of barrier heights, and manifests most obviously as an enhancement of the fusion cross sections at energies near and below the Coulomb barrier. However, the role of nucleon transfer, neck formation and dynamical deformation is less understood and discussion on their effect is relatively scarce as compared to the case of inelastic excitations.^[6]

More than ten years ago, Stelson *et al.*^[7,8] proposed an empirical approach and found that many experimental data can well described by a flat distribution of barriers with the lower-energy cutoff, which corresponds to the energy at which the nuclei come sufficiently close together for neutrons to flow freely between the target and projectile (neck formation). Recently, Zagrebaev^[9] presented a model incorporating neutron transfer in which the intermediate neutron transfer channels with positive Q -values really enhance the fusion cross section at sub-barrier energies.

Wang *et al.*^[10-12] have recently developed an improved quantum molecular dynamics (ImQMD) model. In the framework of the ImQMD model, the dynamical effects such as the excitations of vibration, dynamical deformation, neck formation, isospin, and mass asymmetry of projectile and target, etc., can be simultaneously taken into account. Thus, the microscopic dynamical models such as the ImQMD model offer a useful way to study fusion reactions of heavy ions. With the ImQMD model, Wang *et al.*^[10,11] have studied the fusion reactions of neutron-rich nuclei, es-

pecially for the reactions $^{40,48}\text{Ca}+^{90,96}\text{Zr}$. They found by the detailed calculations that a flow of neutrons occurs between the projectile and target when they come close together, resulting a neck. Consequently, there is a substantial lowering of the dynamic barrier as compared to the static barrier due to the neck formation. As a result, a strong enhancement of sub-barrier fusion cross sections for $^{40}\text{Ca}+^{96}\text{Zr}$ compared to $^{40}\text{Ca}+^{90}\text{Zr}$ have been predicted, which is in good agreement with the experiment.^[13] In addition, they also predict that the neutron-rich reactions $^{48}\text{Ca}+^{90,96}\text{Zr}$ should show even larger sub-barrier enhancement than the $^{40}\text{Ca}+^{96}\text{Zr}$ reaction. The reactions $^{40}\text{Ca}+^{90,96}\text{Zr}$ have been well studied experimentally.^[13] It would be of great interest to measure the fusion cross sections for $^{48}\text{Ca}+^{90,96}\text{Zr}$ in the energy range around the Coulomb barrier to see whether their prediction is fulfilled. In this communication, we report the experimental results of the reactions $^{48}\text{Ca}+^{90,96}\text{Zr}$ and compare the data with the improved calculations for the reactions $^{40,48}\text{Ca}+^{90,96}\text{Zr}$ with the ImQMD model.

The experiments were performed at the XTU Tandem accelerator facility of the Laboratori Nazionali di Legnaro, Italy. Scarlassara F *et al.*^[14] have reported the preliminary experimental results of the reactions $^{48}\text{Ca}+^{90,96}\text{Zr}$ in the International Conference FUSION03. Therefore we briefly describe the experimental procedure here. The targets were $50\ \mu\text{g}/\text{cm}^2$ of isotopically enriched zirconium (99.36% ^{90}Zr and 95.63% ^{96}Zr) which were evaporated on $15\ \mu\text{g}/\text{cm}^2$ carbon foils. A ^{48}Ca beam from the XTU Tandem accelerator was directed at the $^{90,96}\text{Zr}$ targets. The beam energies used were between 139.75 and 176 MeV for the $^{48}\text{Ca}+^{90}\text{Zr}$ reaction and between 133.75 and 170 MeV for the $^{48}\text{Ca}+^{96}\text{Zr}$ reaction, respectively. In both cases, the energy was varied in steps of 1.5 MeV at higher energies and in steps of 0.75 MeV at lower energies. The evaporation residues (ER) were detected at 0° from the beam using an electrostatic deflector^[15]

* Supported by the National Natural Science Foundation of China under Grant No 10235030.

** Email: zhliu@iris.ciae.ac.cn

©2005 Chinese Physical Society and IOP Publishing Ltd

for beam rejection. A further separation is achieved by means of an energy-time-of-flight (TOF) telescope consisting of a microchannel plate and a silicon detector. Four monitor detectors, placed at the angle 15.85° to the beam, are used for absolute normalization, as well as to check the beam quality and angle. The angular distribution of the evaporation residue yield was measured at $E_{lab} = 150, 166$ MeV for both the targets as well as $E_{lab} = 142$ MeV for the ^{96}Zr target alone. The transmission of the electrostatic deflector has been calculated with a Monte Carlo code, which reproduces the transmission measured in the $^{40}\text{Ca}+^{90,96}\text{Zr}$ reactions. It turns out that the transmission is 0.70 ± 0.05 . The experimental cross sections are displayed in Fig. 1 for the $^{48}\text{Ca}+^{90,96}\text{Zr}$ reactions together with the data of $^{40}\text{Ca}+^{90,96}\text{Zr}$.^[13] It can be seen from the figure that the cross sections for the fusion reactions with projectile ^{48}Ca are less enhanced than those of the system $^{40}\text{Ca}+^{96}\text{Zr}$. The much larger enhancement for the case of $^{40}\text{Ca}+^{96}\text{Zr}$ as compared to other three systems clearly indicates that neutron transfer with the positive Q -value should play a significant role in sub-barrier fusion.

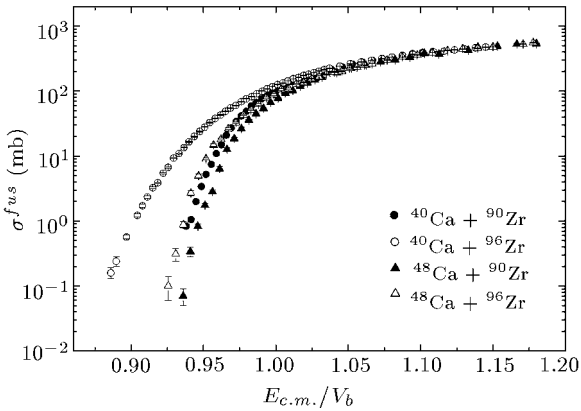


Fig. 1. Experimental excitation functions of the systems $^{40,48}\text{Ca}+^{90,96}\text{Zr}$. The experimental data for $^{48}\text{Ca}+^{90,96}\text{Zr}$ are the measurement of this work. The data for $^{40}\text{Ca}+^{90,96}\text{Zr}$ are taken from Ref. [13].

Scarlassara *et al.*^[14] have analysed the fusion excitation functions and barrier distributions for the systems $^{48}\text{Ca}+^{90,96}\text{Zr}$ in the framework of the coupled channels model. In order to extract the information on the complex dynamical effect, especially the effect of excess neutrons on fusion reactions, in the following we compare the experimental data with the ImQMD model calculations. The ImQMD model is a non-equilibrium transport model which is suitable for studying the dynamical effect in fusion reactions. In the ImQMD model, each nucleon is represented by a coherent state of a Gaussian wave packet

$$\phi_i(\mathbf{r}) = \frac{1}{(2\pi\sigma_r^2)^{3/4}} \exp\left[-\frac{(\mathbf{r}-\mathbf{r}_i)^2}{4\sigma_r^2} + \frac{i}{\hbar}\mathbf{r}\cdot\mathbf{p}_i\right], \quad (1)$$

where \mathbf{r}_i and \mathbf{p}_i are the centres of the i -th wave packet

in the coordinate space and momentum space, respectively. σ_r represents the spatial spread of the wave packet. Here σ_r is dependent on the system size. The expression of σ_r can be found in Ref. [10]. The one-body phase space distribution function for N -distinguishable particles is given by

$$f(\mathbf{r}, \mathbf{p}) = \sum_i \frac{1}{(\pi\hbar)^3} \exp\left[-\frac{(\mathbf{r}-\mathbf{r}_i)^2}{2\sigma_r^2} - \frac{2\sigma_r^2}{\hbar^2}(\mathbf{p}-\mathbf{p}_i)^2\right]. \quad (2)$$

For identical fermions, the approximate treatment of anti-symmetrization is adopted in the ImQMD model by means of the phase space occupation constraint method.^[10,11,16] The propagation of nucleons under the self-consistently generated mean field is governed by the Hamiltonian equations of motion:

$$\dot{\mathbf{r}}_i = \frac{\partial H}{\partial \mathbf{p}_i}, \quad \dot{\mathbf{p}}_i = -\frac{\partial H}{\partial \mathbf{r}_i}, \quad (3)$$

$$H = \int \mathcal{H}(\mathbf{r}) d\mathbf{r}. \quad (4)$$

The energy density functional \mathcal{H} used in this work is the same as that in Ref. [12], which consists of the kinetic and potential energy densities. The potential energy density functional $V_{loc}(\mathbf{r})$ with the Skyrme interaction reads

$$V_{loc} = \frac{\alpha}{2} \frac{\rho^2}{\rho_0} + \frac{\beta}{\gamma+1} \frac{\rho^{\gamma+1}}{\rho_0^\gamma} + \frac{g_{sur}}{2\rho_0} (\nabla\rho)^2 + g_\tau \frac{\rho^{\eta+1}}{\rho_0^\eta} + \frac{C_s}{2\rho_0} (\rho^2 - \kappa_s (\nabla\rho)^2) \delta^2, \quad (5)$$

where $\delta = \frac{\rho_n - \rho_p}{\rho_n + \rho_p}$. The Coulomb energy can be written as a sum of the direct and the exchange contribution and reads

$$U_{Coul} = \frac{1}{2} \int \rho_p(\mathbf{r}) \frac{e^2}{|\mathbf{r}-\mathbf{r}'|} \rho_p(\mathbf{r}') d\mathbf{r} d\mathbf{r}' - e^2 \frac{3}{4} \left(\frac{3}{\pi}\right)^{1/3} \int \rho_p^{4/3} d\mathbf{R}, \quad (6)$$

where ρ_p is the density distribution of protons of the system. The collision term is also included, which plays a very small role in low energy heavy ion collisions. The details of the ImQMD model can be found in Ref. [10].

Table 1. The percentages for pickup $1n, 2n, 3n, 1p, 2p$ channels and stripping $1p$ and $2p$ channels in the reactions of $^{40,48}\text{Ca}+^{90,96}\text{Zr}$ at the incident energy of 3 MeV below the Bass barrier, respectively.

		$^{40}\text{Ca}+^{90}\text{Zr}$	$^{40}\text{Ca}+^{96}\text{Zr}$	$^{48}\text{Ca}+^{90}\text{Zr}$	$^{48}\text{Ca}+^{96}\text{Zr}$
Pickup	$1n$	2.19	5.00	2.14	2.86
	$2n$	0.31	1.07	0.71	0
	$3n$	0	0.36	0	0
Stripping	$1p$	2.81	1.43	0	2.50
	$2p$	0.62	0	0	0
Pickup	$1p$	0.31	0	1.79	0.36

In Ref. [11], the fusion reactions of $^{40,48}\text{Ca}+^{90,96}\text{Zr}$ are studied. The fusion cross sections for $^{40}\text{Ca}+^{90,96}\text{Zr}$

and especially the strong enhancement of sub-barrier fusion reaction for $^{40}\text{Ca}+^{96}\text{Zr}$ are nicely reproduced. However, for even more neutron rich reactions of $^{48}\text{Ca}+^{90,96}\text{Zr}$, the predicted enhancement of sub-barrier fusion cross sections compared with the reaction of $^{40}\text{Ca}+^{96}\text{Zr}$ is not observed in the measurement of this work. In Ref. [11], the enhancement of the fusion cross section for neutron rich reactions was attributed to the dynamical effect of excess neutrons which results in the fast growing of neck leading to the lowering of the fusion barrier. However, it was pointed out in Ref. [11] that the effect of the different shell structure of initial nuclei and the neutron transfer influenced by the structure of initial nuclei might suppress the enhancement effect of the excess neutrons, which were not studied there. Recently, the model proposed in Ref. [9] illustrated that the enhancement of the sub-barrier fusion probability is only for the case of neutron transfer with a positive Q value. In order to dynamically manifest the different effect of the neutron transfer with positive and negative Q values on sub-barrier fusion for neutron-rich systems by means of the ImQMD model, a proper initial condition to make the initial nuclei in the real ground state is of crucial importance. Therefore we make a careful check of the properties of the initial nuclei prepared with the procedure used in Ref. [11]. We find that 600 fm/c for checking the stability of initial nuclei is not enough for ^{48}Ca nuclei. In most cases, the rms radii of ^{48}Ca nuclei prepared increase quickly after 600 fm/c, which means the prepared nuclei are not in the ground state. Clearly, a more rigorous treatment of the initial condition has to be used for correctly study the dynamical process reactions $^{40,48}\text{Ca} + ^{90,96}\text{Zr}$. Thus, in this work, the stability of the initial nuclei is checked within 2000 fm/c instead of 600 fm/c adopted in the works of Refs. [10,11]. Only those prepared nuclei for which the bulk properties and their time evolution are good enough and there is no spurious particle emission within 2000 fm/c are selected as “good initial nuclei” and stored for usage in simulating reactions. Here the reason we take the period of 2000 fm/c for checking the properties of initial nuclei is that the initial nuclei should be stable in a time period long enough compared with the dynamical process of fusion reaction. As a results, much less portion of the pre-prepared initial nuclei can be finally taken to be initial nuclei as compared with that in Refs. [10,11].

Table 2. The corresponding Q values in units of MeV for pickup $1n$, $2n$, $3n$, $1p$, $2p$ channels and stripping $1p$ and $2p$ channels in reactions of $^{40,48}\text{Ca}+^{90,96}\text{Zr}$.

	$^{40}\text{Ca}+^{90}\text{Zr}$	$^{40}\text{Ca}+^{96}\text{Zr}$	$^{48}\text{Ca}+^{90}\text{Zr}$	$^{48}\text{Ca}+^{96}\text{Zr}$	
Pickup	$1n$	-3.608	0.510	-6.825	-2.707
	$2n$	-1.438	5.528	-9.784	-2.818
	$3n$	-5.858	5.240	-18.625	-7.527
Stripping	$1p$	0.159	-0.872	-10.655	-8.358
	$2p$	1.234	2.541	-16.458	-11.823
Pickup	$1p$	-3.944	-10.406	1.277	-1.837

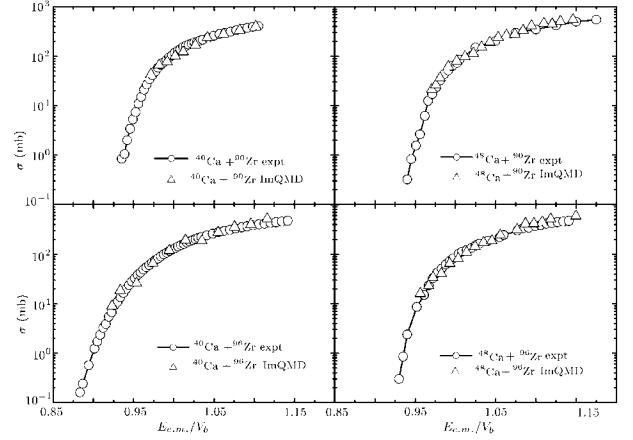


Fig. 2. The fusion cross sections for $^{40,48}\text{Ca}+^{90,96}\text{Zr}$. The open circles denote the experimental data. The triangles denote the calculation results with the ImQMD model, respectively.

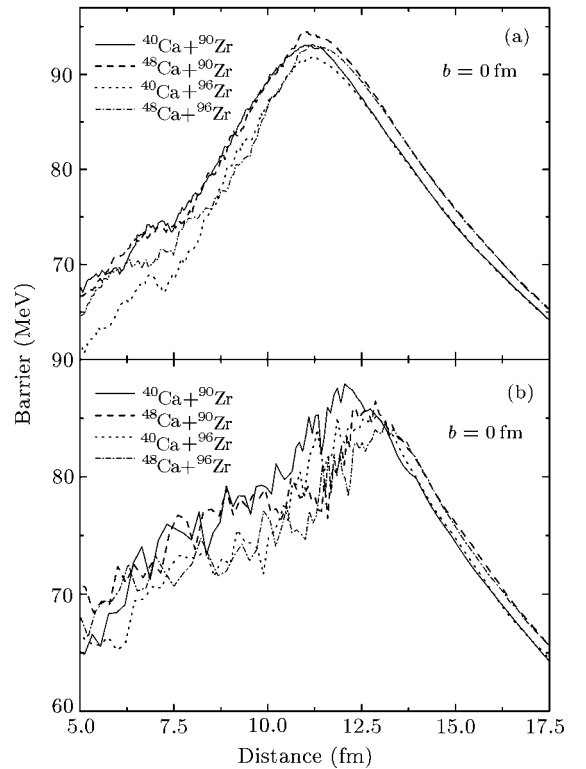


Fig. 3. The dynamic barrier as a function of the distance between the centres of mass of projectile and target for head on reactions of $^{40,48}\text{Ca}+^{90,96}\text{Zr}$ at the incident energy of (a) 5 MeV above and (b) 3 MeV below the Bass barrier, respectively.

Figure 2 shows a comparison of the experimental and calculated fusion cross sections for the systems $^{40,48}\text{Ca}+^{90,96}\text{Zr}$. One can find from Fig. 2 that the experimental results are well reproduced by the ImQMD model calculations. The sub-barrier fusion for neutron rich reaction of $^{40}\text{Ca}+^{96}\text{Zr}$ is substantially enhanced, while for even more neutron rich reactions of $^{48}\text{Ca}+^{90,96}\text{Zr}$ there is less enhancement in the sub-barrier fusion compared with $^{40}\text{Ca}+^{96}\text{Zr}$.

In order to understand the dynamical cause, in Fig. 3 we show the dynamical barriers for head on reactions of $^{40,48}\text{Ca}+^{90,96}\text{Zr}$ at 5 MeV above and 3 MeV below the Bass barrier, respectively. For the case at 5 MeV above the barrier, the reaction of $^{40}\text{Ca}+^{96}\text{Zr}$ encounters a lowest barrier among the four systems. For the case of 3 MeV below the barrier, the reaction of $^{40}\text{Ca}+^{96}\text{Zr}$ again encounters a lower barrier. There is a large fluctuation in the left side of the barrier for the case at 3 MeV below the barrier, and in turn, the accuracy of this part of the barrier for this case is less than the case at 5 MeV above the barrier because of the small cross sections for the sub-barrier fusion. The neutron transfer starts far before the system reaches the top of the barrier. Therefore, the barriers should be strongly affected by the neutron transfer and consequently the reduction of the barrier is closely related to the neutron transfer. Table 1 presents the percentages of $1n, 2n, 3n$, and $1p, 2p, 3p$ transfer in head on reactions of the four systems at 3 MeV below the barrier and the corresponding Q values for nucleon transfer are listed in Table 2 for comparison. The number of reaction events are 320, 280, 280, and 280 for $^{40}\text{Ca}+^{90}\text{Zr}$, $^{40}\text{Ca}+^{96}\text{Zr}$, $^{48}\text{Ca}+^{90}\text{Zr}$ and $^{48}\text{Ca}+^{96}\text{Zr}$, respectively. The pick up $1n, 2n, 3n$ channels are strongly enhanced for reaction of $^{40}\text{Ca}+^{96}\text{Zr}$ compared with other three reactions. Figure 4 shows the time evolution of the neck width for fusion reactions of $^{40}\text{Ca}+^{90}\text{Zr}$, $^{40}\text{Ca}+^{96}\text{Zr}$, $^{48}\text{Ca}+^{90}\text{Zr}$ and $^{48}\text{Ca}+^{96}\text{Zr}$ at $E_{CM} = 93, 95$ MeV and impact parameter $b = 0$, respectively. From Fig. 4 we can see that the neck grows faster for $^{40}\text{Ca}+^{96}\text{Zr}$ than other three systems. The quicker the neck grows, the stronger the reduction of the barrier is. We therefore can attribute from this

calculation that the reduction of the barrier encountered by $^{40}\text{Ca}+^{96}\text{Zr}$ is due to the strong dynamical effect of the neutron transfer, which leads to the enhancement of the sub-barrier fusion cross section for $^{40}\text{Ca}+^{96}\text{Zr}$. While for even neutron rich reactions of $^{48}\text{Ca}+^{90,96}\text{Zr}$, the reduction effect of excess neutrons on the barrier is suppressed due to the negative Q value for neutron transfer leading to less enhancement of the sub-barrier fusion cross sections compared with non-neutron-rich reaction of $^{40}\text{Ca}+^{90}\text{Zr}$.

In summary, the fusion cross sections for $^{48}\text{Ca}+^{90,96}\text{Zr}$ around the Coulomb barrier have been measured. The experimental results of $^{40,48}\text{Ca}+^{90,96}\text{Zr}$ are compared with the improved quantum molecular dynamics model calculations. It is shown in comparison that neutron transfer starts far before the system reaches the top of the barrier and the flow of neutron between the reaction partners results in the neck formation. Consequently, the fusion barriers are strongly affected by the neutron transfer. Our calculations indicate that the neck grows faster for $^{40}\text{Ca}+^{96}\text{Zr}$ than other three systems, resulting in a stronger reduction of the barrier. We therefore can attribute from this calculation that the reduction of the barrier encountered by $^{40}\text{Ca}+^{96}\text{Zr}$ stems from the strong dynamical effect of the neutron transfer, which leads to the enhancement of the sub-barrier fusion cross section for $^{40}\text{Ca}+^{96}\text{Zr}$.

References

- [1] Dasso C H et al 1983 *Nucl. Phys. A* **407** 381
Dasso C H et al 1983 *Nucl. Phys. A* **407** 221
- [2] Rowley N, Satchler G R and Stelson P H 1991 *Phys. Lett. B* **254** 25
- [3] Wei J X et al 1991 *Phys. Rev. Lett.* **67** 3368
- [4] Dasgupta M et al 1998 *Ann. Rev. Nucl. Part. Sci.* **48** 401 and references therein
- [5] Hagino K et al 1999 *Comput. Phys. Commun.* **123** 143
- [6] von Oertzen W and Krouglov I 1996 *Phys. Rev. C* **53** R1061
- [7] Stelson P H 1988 *Phys. Lett. B* **205** 190
- [8] Stelson P H et al 1990 *Phys. Rev. C* **41** 1584
- [9] Zagrebaev V I 2003 *Phys. Rev. C* **67** 061601(R)
- [10] Wang N, Li Z X and Wu X Z 2002 *Phys. Rev. C* **65** 064608
- [11] Wang N, Wu X Z and Li Z X 2003 *Phys. Rev. C* **67** 024604
- [12] Wang N, Li Z X, Wu X Z, Tian J L and Liu M 2004 *Phys. Rev. C* **69** 034608
- [13] Timmers H, Ackermann D, Beghini S, Corradi L, He J H, Montagnoli G, Scarlassara F, Stefanini A M and Rowley N 1998 *Nucl. Phys. A* **633** 421
- [14] Scarlassara F, Montagnoli G, Beghini S et al 2004 *Prog. Theor. Phys. Suppl.* **154** 31
- [15] Beghini S, Signorini C, Lunardi S et al 1985 *Nucl. Instrum. Methods A* **239** 585
- [16] Papa M, Maruyama T and Bonasera A 2001 *Phys. Rev. C* **64** 024612

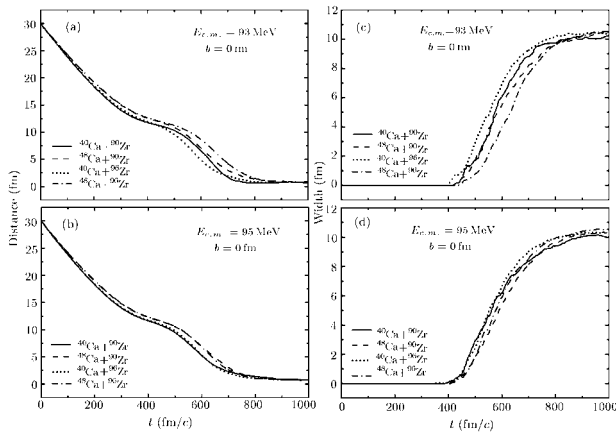


Fig. 4. The time evolution of the distance and neck width for head on reactions of $^{40,48}\text{Ca}+^{90,96}\text{Zr}$ at $E_{CM} = 95, 93$ MeV, respectively.